The C_3 molecule: A Literature Study and Spectroscopic Investigations in Flames and on Graphite

Gunnar Larsson

Lund Reports on Combustion Physics

LRCP-82
2002

Lund Institute of Technology
Sweden

The C_3 molecule: a literature study and spectroscopic investigations in flames and on graphite

Gunnar Larsson

Lund reports on Combustion Physics, LRCP-82

Division of Combustion Physics
Lund Institute of Technology
Box 118
S-221 00 Lund
Sweden

TABLE OF CONTENTS

Abstract

The potential of C_3-spectroscopy as a mean of measuring soot concentrations is investigated. By first vaporizing soot and then taking laser-induced fluorescence (LIF) spectra it should in principle be possible to monitor the soot content.

A detailed literature study is presented about C_3 spectroscopy. The molecular structure is described as well as the thermodynamical and chemical properties. Recent work dealing with C_3 spectroscopy as a method to quantitatively observe C_3 concentrations is presented.

The experimental study was directed towards the vaporization of graphite and soot in flames to create C_3 fragments. Laser-induced fluorescence was used to study the fragments. An excitation beam with a wavelength of 405 nm was used to excite C_3 on the A-X transition. To vaporize the soot a vaporization beam with energies up to 50 mJ was used. These beams were separated in time by 10 nanoseconds.

Laser-induced fluorescence was used in two ways, fluorescence spectra and excitation scans. In the first a single excitation wavelength was used and a spectrum taken, in the latter the excitation wavelength was scanned and the total fluorescence monitored. Both laser-induced fluorescence spectra and excitation scans, were taken in a flame and on graphite. A photomultiplicator, together with interference filters, was used to collect the signal in the excitation scan, while a CCD-camera with long-pass filter was used when fluorescence spectra were recorded.

The flame used was a welding torch. Excitation at 405 nm gave no observable signal from C_3. Laser-induced incandescence, i.e. blackbody radiation from heated soot particles, was seen, as well as laser-induced fluorescence from C_2 and CH. Graphite was used because the similarities in structure with soot. As in flame, no C_3-signals were observed in graphite. The use of graphite posed many problems with reflections. A signal, which may be attributed to PAH, was observed as a consequence of vaporization of graphite.

1. Introduction

The first known observation of C_3 was reported 1881 when Huggins observed lines around 4050 Å in a spectrum from the comet b 1881 [1]. In 1942 it was for the first time reported as observed in laboratory by Herzberg as a result of discharges through methane. However, he suggested it to be CH_2 [2]. By substituting the hydrogen in methane with deuterium Monflis and Rosen could 1949 show this assignment to be incorrect [3]. In 1951 Douglas could identify the molecule as probably being C_3 by using ^{13}C [4].

Although identified since over 50 years, spatial measurements of C_3 in laboratory are a relatively new phenomenon. The progress is closely related to research in mainly two fields: the creation of fullerenes and investigations of the processes that occur in diamond deposition. In 1996 Raiche and Jeffries published measurements of spatial distributions in diamond deposition [5] and in 1997 by Luque et al. published further results in the same field [6]. In 2000 Takizawa et al. made measurements in a C_4F_8-plasma [7]. Sasaki et al. has recently published results of two-dimensional laser-induced fluorescence from laser ablation of graphite targets [8].

C_3 was first observed in a comet and over one hundred papers have been written, in scientific publications, on comets that contain C_3. It has later been found in other astronomic objects such as in the atmosphere of cool carbon stars, in the circumstellar shells of super giant stars [9] and recently in interstellar clouds [10]. On earth, it has been detected in the emission from acetylene-oxygen flames [11]. Several different, intended or not, methods for creating C_3 have been used. Among the most common are laser-induced vaporization of graphite rods and electric discharges of carbon-containing gases. A lot of investigations, both theoretical and experimental, have been made in the late 80s and in the 90s. In 2001, to my knowledge, the first two-dimensional laser-induced fluorescence (2D-LIF) of C_3 was done as a result of laser ablation of graphite. Reviews of the up to date knowledge of C_3 and other small carbon clusters were published by Weltner and van Zee in 1989 [9] and by van Orden and Saykally in 1998 [12].

The objective of this study is to explore the potential of measuring soot using laser-induced fluorescence of C_3, created from laser-vaporized soot. Non-intrusive measurements of soot are important in order to gain understanding of combustion processes. A high concentration of soot indicates inefficient combustion and soot is created in carbon rich combustion at high temperature. If soot remains in the exhaust gases it could cause health effects and decreased visibility. It is difficult to measure soot content since soot is no molecule and therefore cannot be monitored by usual spectroscopic methods. In contrast to molecules soot do not have any transitions that could be used as identifiers. To identify soot we therefore need to use either the chemical content of soot vapor or the physical properties of soot particles as markers. If measurements are made on soot vapor it is possible to use the same spectroscopic methods as for other molecules. Blackbody radiation and absorption are physical phenomena used to measure soot concentrations.

Since C_3 is the major constituent in graphite vapor and soot consists to 90 % of carbon in a graphite-like structure, it has been proposed as an indicator of soot [13]. The proposed advantage of C_3 over C_2 should be lower background and higher concentration. C_2 has an intense spontaneous emission in many flames and this could interfere with the results. An example of this is the blue-green light that could be seen around the wick in an ordinary candle. This light comes from C_2. The second advantage is that vaporized soot is expected to contain more C_3 than C_2 at the temperatures to which the soot is heated, about 4 500 K [14].

2. Molecular physics of C_3

2.1. The ground transition

The ground transition of C_3 has a wavelength of 405 nm and is an A $^1\Pi_u^+$-X $^1\Sigma_g^+$ transition. A spectrum for this transition is given in Figure 1. The C_3 molecule is built up by σ- and π-orbitals. The π-orbitals consist of atomic p_x- and p_y-orbitals, which in a molecule is directed perpendicular to the bonding axis. They do therefore allow bending. On the opposite σ-orbitals, which consist of s- and p_z-orbitals, have a probability distribution that is symmetric around the bonding axis and do not allow bending.

In the ground state is the C-C distance 1.299 Å, independent of bending [9]. The reason for the independence is that no π_g–orbitals are populated in this state, making it possible for the molecule to bend without disturbing the C-C bonding. When the molecule is excited the π_g-orbital is populated, as seen in Table 1. This causes the bending frequency to rise and is also the cause of the strong Renner-Teller effect, described below, in the upper state. The same behavior is seen in many molecules. The transition strength has in experiments been measured to be twice as high as in theory; this inconsistence between theory and experimental results is still to be explained [9, 16].

Table 1. Populated orbitals for the electronic states in C_3 [15].

Electronic state	Outer orbitals
$X\ ^1\Sigma_g^+$	$4\sigma_g^2 3\sigma_u^2 1\pi_u^4$
$A\ ^1\Pi_u$	$4\sigma_g^2 3\sigma_u 1\pi_u^4 1\pi_g$
$^1\Pi_g$	$4\sigma_g 3\sigma_u^2 1\pi_u^4 1\pi_g$
$^1\Delta_u$ och $^1\Sigma_u^+$	$4\sigma_g^2 3\sigma_u^2 1\pi_u^3 1\pi_g$

Between different experiments on C_3 it happens that different lines are observed in the same part of the spectrum. As an example of this, Baker et al. observed stretching vibrations, but not bending vibrations, in the same part of the spectra where Balfour et al. observed bending, but not stretching vibrations [17]. Since Baker et al. even in their experiment in 1993 did not see bending vibrations using the same method, electric discharge through CO; this indicates that different methods result in population of different vibrational levels [17, 18].

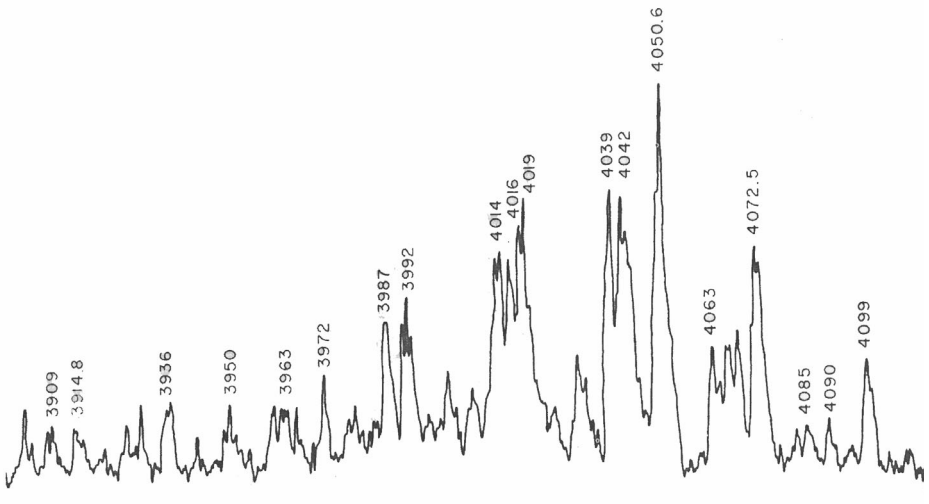

Figure 1. C_3-spectrum from the comet Ikeya [19].

2.2. Thermodynamic and Chemical Properties

Since the method used is based on measurements of vaporized soot we need to know the content of vaporized soot, especially the amount of C_3. This is not known very well and therefore as a substitute we can look on the vapor of carbon/graphite. From theoretical and experimental data it is known that C_3 constitutes the largest fraction of the carbon vapor in at least the temperature interval 2 000-10 000 K. It should be noted that even if the partial amount of C_3, shown in Figure 2, decrease when the temperature increase over 4 000 K the total amount increase since more carbon is vaporized [14].

The values are from equilibrium calculations and may therefore not correspond to the actual measuring situation. The process of formation of C_3 is probably of the form $C + C + M \rightarrow C_2 + M$ and $C_2 + C + M \rightarrow C_3 + M$. It has been reported that as an effect of this it takes about 10-100 μs until C_3 is created when vaporizing graphite by a laser under low pressures, up to 5 Torr [8]. Since the molecular collision rate is inversely proportional to the pressure it should be correspondingly shorter. That C_3 is created by recombination of carbon atoms is an idea that is suggested also by Baker [18]. It takes about 5-10 ns to create C_2 in vaporization of soot in an ordinary flame [20].

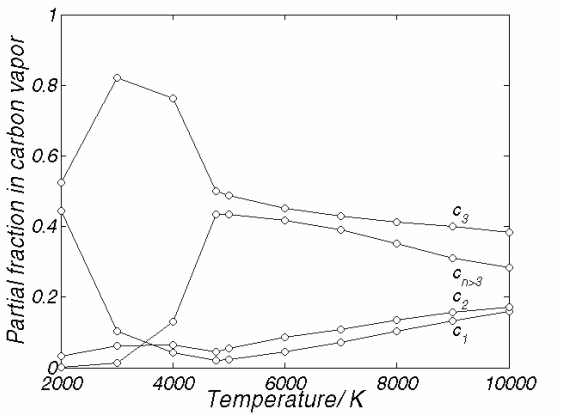

Figure 2. Composition of carbon vapor at different temperatures [14].

Ortman et al. have investigated chemical reactions in carbon vapor [21]. Nelson et al. investigated chemical reactions with alkanes, alkenes, alkynes and allenes in 1981 and 1982 [22, 23]. They found reactions with alkenes, alkynes and allenes, but not with alkanes. When adding methyl groups on a compound the reaction speed increased and the activation energies decreased. C_3 has been purposed as a growth element in soot formation [24].

2.3. Geometry

The first analysis of the spectrum indicated that it was linear both in the ground level, $X\ ^1\Sigma_g^+$ and in the excited level, a $^1\Pi_u$. Until the mid-sixties it was supposed that C_3 was a linear molecule, but in 1965 Gausset et al. realized the possibility that it might not be linear, but in that case the potential function must be rather flat. Since then there has been contradicting measurements and theoretical calculations.

Weltner and van Zee suggest a quasi-linear structure in their review [9]; van Orden and Saykally suggest a linear structure, although very flat. When anti-symmetrically excited a barrier to linearity appears, which becomes stronger when it is further excited. In opposition, when symmetrically excited it gets more rigidly linear [12].

In case it is quasi-linear the barrier to linearity has been calculated to be 16.5 cm^{-1} and the bond angle to be 162.5° [9]. Measurements by Northrup and Sears suggest the barrier to linearity to be even lower, although they find other reasons to believe C_3 to be quasi-linear [25]. The low bending frequency has as result that bending angles as large as 60° are possible, which are to large to be treated as small bendings [9].

2.4. Transition rules and transition strength

In order to investigate a molecule it is important to know what transitions are allowed. This is more difficult for polyatomic molecules than for atoms and diatomic molecules. To make the description of polyatomic systems easier we can use **group theory**. Group theory is a way to,

in general terms; describe what happens with a system when it is rotated, mirrored, inversed etc. This is of use since systems that behave the same under these changes also share common electronic, vibrational and rotational properties since they behave the same under these changes.

When using group theory two terms have to be grasped, **group** and **specie**. A **symmetric group** is an arrangement of objects, in this case atoms, and the relation between these, i.e. which atom is bound to which. Each symmetric group allows a number of symmetric operations such as rotation and mirroring and is, if the initial conditions are the same, also affected in the same way. This means that we can generalize all diatomic molecules to one case, all linear tri-atomic molecules to another case and all bent tri-atomic molecules to yet another. The symmetric group gives the template and the rules for the symmetric specie.

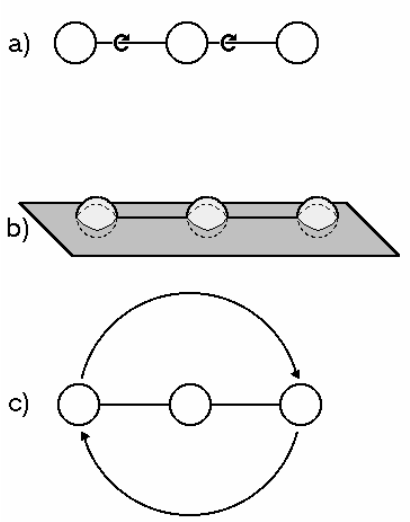

Figure 3. Symmetric properties of C_3 used to identify its symmetric group.

In its linear state C_3 belongs to the symmetric group $D_{\infty h}$. The reasons for this are shown in Figure 3. Because it is linear, it has an infinite number of symmetry angles, i.e. you can rotate the molecule how much you want around its own axis, it will still looks the same (see Figure **3a**). This is indicated with the infinity sign. The h indicates that it has a horizontal symmetry plane perpendicular to this plane (see Figure **3b**). The D indicates that in the other plane of symmetry the molecule has two-fold symmetry, i.e. you can rotate it 360/2=180° and it will retain its shape (see Figure **3c**) [26, 27].

The **symmetric specie** is the actual case. It answers questions such as which is the shape of the potential, is it possible to mirror it without changing its shape, is it possible to rotate it or invert it without changing its shape.

To know this we have to know the symmetry for each electronic orbital, as well as from vibrational and rotational levels. In this case we have help of the fact that the symmetry of a filled shell sum up to the basic specie for that symmetry. This results from the fact that if all orbitals in a shell are filled there will be no change if we for example rotate the system so that each orbital take the place of the old one. All orbitals are anonymous since we cannot differ one orbital from another. This will no longer be the case when not all orbitals are filled since now there is something that could identify the orbital. We therefore only need to know the orbitals that not are part of a full shell.

For the first electronic state we have is Σ_g^+. Σ indicates the lowest symmetric level, and also that the orbital angular momentum is zero. The labeling of the symmetric specie and the orbital angular momentum is the same. The labeling for different symmetries differs between symmetric groups, since the possible states differ. The linear symmetric group uses the same nomenclature as for diatomic molecules. The reason behind this is that the diatomic molecule is a linear molecule. Historically the nomenclature for diatomic molecules was invented first and it was seen practically preferable to make the nomenclature for the linear symmetric group consistent with the already existing for diatomic molecules.

The Σ_g^+ level has no angular momentum since the only orbital that contains any angular momentum, π_u, is full. In Π and Δ electronic states we have, as seen in Table 1, π orbitals that are not in full shells and they can therefore form other states. The g comes from the german word *gerade*, i.e. even, which means that the molecule will retain its shape when it is inverted; and + because it has even parity when reflected.

The symmetry of the electronic states is not enough; we also have symmetry from vibration and rotation. The vibrational species for the respective vibrations are [26]:

v_1: Σ^+
v_2: Π
v_3: Σ^+

The general rule for vibrational transitions are that they can only take place between levels with the same vibrational specie; another way to express this is that the direct product of the upper and lower state should be symmetric. For anti-symmetrical vibrations this could be simplified. In this case the quantum number could only change by even numbers. If many anti-symmetric vibrations are excited this applies to the sum, the individual vibrations could change by odd numbers, since it is the symmetry of the entire molecule we are interested in, not of each vibration. In general only band for which the vibrational quantum numbers do not change are strong. In C_3, however, the bending frequency is so low that that even other bands exist, because the low bending frequency has as effect that the Boltzmannfactor does not decrease as fast as usual.

When the molecule becomes rotationally excited every single excitation change the sign of the molecule, i.e. it is dependent on J as $(-1)^J$. This has as result that for a vibronic level, which is positive in its ground state only even rotational excitations are allowed, while the opposite is the case when it is negative in its ground state. This could be changed if the nucleus of the molecule has a spin. In this case the nuclear spin may orient in a number of different directions, resulting in different molecules having different total nuclear spin and therefore different allowed and forbidden transitions. This will in a measurement show up as some lines being stronger, since they are allowed when the nuclei spin has a probable distribution, while other lines are weaker, allowed by less probable distributions. The carbon nucleus has no spin, and therefore C_3 is not affected. Because of the l-type doubling explained below each rotational level will split into two, for vibrational levels higher than Σ. These levels have opposite sign. As example, for rotations with J=0,1, and 2 we will, if we have a positive groundstate, instead of +, -, + have (+-), (-+), (+-) as symmetric signs.

Not only electronic states, as well as vibrational and rotational bands, but also the spin has symmetric species. In $D_{\infty h}$ symmetry we have for spin S=0 the symmetric sign Σ_g^+ and for S=1 Σ_g^- and Π_g.

When merging two or more functions with some kind of symmetry, the laws and groups of direct product is applied. This is the case when we investigate the symmetry for the entire molecule, which is the product of the electronic, vibrational and rotational parts of the wave function. The direct product of two symmetries is more or less as ordinary multiplication; except that here do multiplication tables really serve a practical purpose. The direct product could often generate more than one symmetric specie as result, i.e. the new function may fit many symmetries. The lower direct products in $D_{\infty h}$ symmetry are viewed in Table 2.

Table 2. Direct Products for $D_{\infty h}$-symmetry [26, 27]. The direct product shows the symmetry of a system, which is built up by two different symmetrical components, as example the components from the electronic symmetry and the vibrational symmetry in a molecule.

	Σ^+	Σ^-	Π	Δ	Φ
Σ^+	Σ^+	Σ^-	Π	Δ	Φ
Σ^-		Σ^+	Π	Δ	Φ
Π			$\Sigma^+, \Sigma^-, \Delta$	Π, Φ	Δ, Γ
Δ				$\Sigma^+, \Sigma^-, \Gamma$	Π, H
Φ					Σ^+, Σ^-, I

In all transitions the symmetry of the total system must stay unchanged when a photon cause a transition. This is a simplification from the fact that the potential functions must overlap, since the transition probability otherwise is zero. It can be shown that this is only the

case if the system preserves its symmetry. This rule is the general rule for all transitions, and from it the rules for allowed transitions can be drawn for all kind of molecules. Only transitions between states with the same spin are allowed, because otherwise the spin functions are orthogonal to each other, which have as effect that potential functions do not overlap.

It is not only possible to assign symmetric properties to the molecule. It is also possible to assign a symmetric specie for an incoming photon in the same way that we can assign symmetric species to the orbital of the molecule. In the symmetry of a linear molecule, the photon contains the two symmetric species Σ^+ or Π. This has, as effect that transitions only can take place between electronic states that generate a direct product that is Σ^+ or Π, since otherwise the symmetry of the total system would change.

Except for the group theoretic description of the molecules it is also often of importance how many independent movements of inertia a molecule has. Therefore molecules are labeled spherical tops, symmetrical tops, asymmetrical tops or linear molecules according to the number of independent movements of inertia. Spherical tops have all three equal movements of inertia equal, in symmetrical tops two are equal, but the third differ, and in asymmetrical tops all three movements of inertia are different. Linear molecules, such as C_3 can be seen as a special case of the symmetrical top since two of the movements of inertia are identical. The difference is that the third, the one around the axis of the molecule, in this case is zero.

2.5. Vibrational and Rotational bands

2.5.1. Vibrational bands

The number of vibrational modes for a molecule depends on the number of atoms. An atom has three degrees of freedom, i.e. three independent variables are needed to describe the atom. C_3 contains three atoms and has as a consequence nine degrees of freedom. Three of those are needed to describe the place in space for the molecule, three more could be use to describe rotations of the system around the three axis. In a linear molecule only two rotations are possible, since rotation around the axis of the molecule does not change any coordinate. The two remaining rotations are degenerate since they are physically indistinguishable. This leaves us with four degrees of freedom left for vibrations. The name of these vibrations are symmetric stretch, bending and anti-symmetric stretch. The bending vibration is degenerate which accounts for the fourth degree of freedom. The reason for this degeneracy is the same as for the rotational degeneracy; the linear structure makes the bending vibrations indistinguishable. These three vibrations are given the quantum numbers v_1, v_2 and v_3, while the vibrational constants, representing the energy need to add one vibrational quantum, are labeled ω_1, ω_2 and ω_3 and shown in Table 3.

Table 3. Vibrational constants for the electronic states of C_3. The source for each value is given inside the brackets.

	ω_1		ω_2		ω_3	
X $^1\Sigma_g^+$	1226	[19]	63,5	[19]	2 040	[19]
A $^1\Pi_u^+$	1089,9	[28]	311,1	[28]	563	[28]
$^1\Sigma_u^+$	1080	[29]	300	[29]	780	[29]
a $^3\Pi_u^+$	1154,2	[30]	505	[31]	1455,3	[30]
b $^3\Pi_g^+$			345	[31]		
$^1\Delta_u$ /$^1\Pi_g$	940	[32]	168	[32]		

One of the most special characters of C_3 is the very low bending frequency, 63 cm^{-1}, in the ground state. The low bending frequency is the cause of other phenomena in the C_3-molecule such as the large l-type doubling [19]. In the upper state of the ground transition, i.e. A $^1\Pi_u^+$, the bending constant increase to 311.1 cm^{-1}. This large change in bend frequency is attributed the fact that a π_g-orbital, which is anti-bonding, becomes occupied.

Also the anti-symmetric stretch constant, ω_2, for the lower state, 2040.0 cm^{-1}, is well known since many years. This is not the case for the upper state, which has been a subject of a lot of

theoretical discussions and experiments with different results. In the 90s there have been indications that it is lower than earlier expected. Izuha and Yamanouchi have in 1995 and 1998 measured it to be 541.7 and 539.4 cm^{-1} [33, 34]. This in contrast to earlier values around 800 to 900 cm^{-1}.

The vibrational quantum numbers do together with the vibrational frequencies given in Table 3 give an approximate description of the molecule as long as the harmonic oscillator is an accurate description of the vibrations. A more specific description of the vibrational states is [13]:

$$G(v_1 00) = 1229{,}7v_1 - 6{,}08v_1^2 \quad (2.1)$$

$$G(0v_2 0) = 61{,}94v_2 + 2{,}53v_2^2 - 0{,}0271v_2^2 \text{ for } l_2=0 \quad (2.2)$$

$$G(00v_3) = 2058{,}5v_3 - 20{,}15v_3^2 \quad (2.3)$$

where v_1,v_2 an v_3 are the quantum numbers for symmetrical stretching, bending, and anti-symmetrical stretching. Except for the anharmonicity shown above, there is also a strong coupling between the bend- and stretch vibrations, where the bending constant gets higher the more stretching we have. This is not the case for anti-symmetric stretching vibrations where excitation lowers the bending constant slightly [13].

2.5.2. Rotation bands

The rotational energy is given by:

$$F_v(J) = B_v\left[J(J+1) + K^2\right] - D_v\left[J(J+1) - K^2\right]^2 \pm q\left[J(J+1)\right] \quad (2.4)$$

where J is the rotational quantum number, B_v is the rotational constant, D_v the centrifugal distortion constant and q the l-type splitting constant. There is quite large anharmonicity and Gausset et al. fitted the rotational constant for the ground level with function 2.5.

$$B_{0v_2 0} = 0{,}4305 + 0{,}0122v_2 - 0{,}00077v_2^2 \quad (2.5)$$

where the second value comes from a large anharmonicity [9], while the last is the result of a strong l-type doubling [19], discussed below. The fit does however not fit all data very well. This is because we in many cases have perturbations by other electronic states. The interaction between rotations and vibrations also influence the rotational constant, which Northrup and Sears [25] have by fitted function 2.6:

$$B_v = B_e - \alpha_1(v_1 + 1/2) - \alpha_3(v_3 + 1/2) - \alpha_2(v_2 + 1) - \gamma_2(v_2 + 1)^2 - \delta_2(v_2 + 1)^3 \quad (2.6)$$

$$\alpha_2 = -0{,}01066\, cm^{-1} \quad (2.7)$$

$$\gamma_2 = -0{,}00341\, cm^{-1} \quad (2.8)$$

$$\delta_2 = -0{,}00000438\, cm^{-1} \quad (2.9)$$

$\alpha_{1,2,3}$ is the vibration-rotation interaction constant for each vibration, γ_2 and δ_2 is higher order polynomial fit coefficients; α_1 and α_3 were not measured. From Baker [18] we get a value α_1=–0.0038 in the ground state. Izuha and Yamanouchi get, without using the correction constants γ and δ, the values α_1=0.005(4), α_2=-0.0027(9) and α_3=-0.0133 [33].

In the upper state, A $^1\Pi_u$, is the rotational constant 0.4146 cm^{-1} with a vibration-rotation interaction constant of 0.0035 cm^{-1} [18]. The distortion constant is $-7.42*10^{-7}$ cm^{-1} in the ground level [9].

2.6. Combinational and perturbing effects

2.6.1. l-type doubling

For linear molecules we do in general have degeneracy in l. Since there is no physical difference between when a linear molecule rotates right or left both +l and –l would have the same energy. There are, however, times when this is not true, in those cases we have l-type doubling.

There are two reasons for l-type doubling. First, when the bending vibration is excited the molecule bends and becomes more and more an asymmetric top. For asymmetric tops we have no degeneracy for the same absolute values of l, since rotating left or right has a physical meaning for an asymmetric top. Second, we have the Coriolis force. When a rotating object is moving away from the center it seems to slow down. If it on the other hand encloses the center it seems to accelerate. In a molecule we have this case when we have anti-symmetric stretching, in this case the center nucleus moves closer to one of the outer nuclei but away from the other. In perspective of the other nuclei it will therefore accelerate respectively retardate, causing the molecule to bend.

The l-type doubling is given by:

$$\Delta v = qJ(J+1) \tag{2.10}$$

where v is the split in cm^{-1}, q the l-type doubling coefficient, J the rotational quantum number. The size of the l-doubling constant is for a linear molecule:

$$q_{v_2} = \frac{B^2}{\omega_2}\left(1 + \frac{4\omega_2^2}{\omega_3^2 - \omega_2^2}\right)(v_2 + 1) \tag{2.11}$$

where ω_2 and ω_3 are the vibrational constants and B the rotational constant. When the bending vibration is excited once, v_2=1, the l-type doubling is 0.0055 cm^{-1} [19]. The large l-type doubling is therefore, as could be seen from eq. 2.11, a result of the low bending frequency constant, ω_2.

2.6.2. l-type resonance

The l-type resonance is a result of the sub states lying close together. According to Gausset et al. there is l-type resonance in C_3, and as a result the 020-vibrational level consists of two close laying Σ_g^+ states [19]. This is agreed by Kawaguschi et al. [35] but not by Rohlfing [13] and Balfour et al. [36]. Rohlfing states that the molecule could be well described without l-type resonance, and that the 020-vibrational level consists of a Σ_g^+- and a Δ_g-state as usual [37]. Because the two sub-states should lie so close to each other they will perturb each other, this results in that at high J-values the second component of Δ_g is pushed up while Σ_g^+ is pushed down [19].

2.6.3. K-type doubling

Vibrations do create rotation, which is described by the quantum number l

$$l = \left| \sum_i (\pm l_i) \right| \tag{2.12}$$

where l=0,1,2,… corresponds to Σ, Π, Δ, … vibrational states and i is the index for each electron. This couples with the electronic orbital angular momentum (Λ) to

$$K = \left| \pm \Lambda \pm l \right| \tag{2.13}$$

where K=0,1,2,.. corresponds to Σ, Π, Δ, … vibronic states.

For symmetric tops J- and K-values are well defined. This is not the case for asymmetric tops. Therefore, when we move from a perfect symmetric top to an asymmetric top the K-values split up, this splitting is called K-type doubling and has no good quantum number [26]. In linear molecules only l- or Λ-type doubling can cause K-type doubling [37]. The doubling is proportional to $J^{n-1}(J+1)^{n-1}$, where n stands for the vibronic state number, which is one for Π, two for Δ etc. [37].

2.6.4. Renner-Teller effect

In a zero-approximation levels with the same vibronic state has the same energy, i.e. the electronic angular momentum do not interact with the vibrational angular momentum. In reality this is not always the case, especially not for C_3.

The splitting between these levels is called the Renner-Teller effect. When the molecule is bent, i.e. when the bending vibration is excited, the potential function splits in two. In symmetric terms this has the effect that the symmetric group is changed from $D_{\infty h}$ to D_{2h}. The symmetric species Π_g splits into A_2 and B_2, Π_u to A_1 and B_1, Δ_g to A_1 and B_1, and Δ_u to A_2 and B_2 in this new symmetry. These components are sometimes referred to as $\Pi^{(+)}$ and $\Pi^{(-)}$ etc., where the sign indicates the level with the higher and lower energies. Which symmetry term that corresponds to each energy level is difficult to know since the both potential functions touch each other and the electron therefore can go from one to another.

It has as effect that the bending vibration is split, for v_2=1 it results in Σ_g^+,Δ_g and Σ_g^- sub states. The energy levels that the Renner-Teller effect gives rise to can be calculated from the formulas:

When $K = 0$ (Σ vibronic states):

$$G(v_2, K) = \omega_2 (v_2 + 1)\sqrt{1 \pm \varepsilon} \tag{2.14}$$

When $K \neq 0, v_2 = K - 1$ (lowest single vibronic level of Π, Δ, …):

$$G(v_2, K) = \omega_2 \left[(v_2 + 1) - \frac{1}{8}\varepsilon^2 K(K+1) \right] \tag{2.15}$$

When $K \neq 0, v_2 > K - 1$ (remaining Π, Δ, …):

$$G(v_2, K) = \omega_2 (v_2 + 1)(1 - \frac{1}{8}\varepsilon^2) \pm \frac{1}{2}\omega_2 \varepsilon \sqrt{(v_2 + 1)^2 - K^2} \tag{2.16}$$

In the case of C_3 we have ε = 0.537 which is one of the strongest Renner-Teller effects observed [9].

2.7. Electronic bands

Up to date at least six electronic levels are found in C_3. Except for X $^1\Sigma_g^+$ and A $^1\Pi_u^+$, already discussed, we have one singlet band $^1\Sigma_u^+$ and two triplet bands, a $^3\Pi_u$ and b^3 Π_g, and apart from this at least one band which lack a final identification.

Weltner and McLeod first identified the **a $^3\Pi_u$** band in 1964 [37]. They found peaks at 585.6 and 590.5 nm when exciting at 365.0 or 404.7 nm in neon and argon [37]. It is spin forbidden to deexcite to the ground level, and is therefore metastable [30]. The state has a lifetime of 20 ms [37]. A strong Renner-Teller effect is seen in this level, which also is the case for the **b$^3\Pi_g$** band. Only bands between the same vibrational levels are seen between this level and a^3 Π_u [38].

In 1982 Chang and Graham detected the $^1\Sigma_u^+ \rightarrow {}^1\Sigma_g^+$ transition at about 1890 Å. It is created by a strongly bonding π_u that is excited to an essentially nonbonding π_g-orbital. This results in a lengthening of the bonds, which in turn lowers the stretching frequencies [30]. The transition is theoretically calculated to be at wavelengths around 155 nm and very intense [15]. Since Chang and Graham could not measure such low wavelengths this identification was for many years doubtful. Recently Monninger et al. have, however, detected this transition over a broader interval and verified the identification. The band has a large spectral range from 1900 Å down to at least 1400 Å. The spectrum could be seen in Figure 4. The peak around 1 400 Å is also likely to come from C_3, it is, however, yet unassigned [40].

In 1989 Lemire et al. found a new weak electronic band, which still is unidentified. It is a result of a dipole forbidden transition to either **$^1\Pi_g$** or **$^1\Delta_u$**. The transition is in the region 266-302 nm [41], where the most prominent peak is near 281.2 nm [32]. The reason we can see it is because it gain oscillator strength from the transition $^1\Sigma_u^+$-X $^1\Sigma_g^+$ and $^1\Pi_u$-X $^1\Sigma_g^+$ by the Herzberg-Teller mechanism [32]. Due to the large displacement in bond length Izuha and Yamanouchi suggested it to be $^1\Delta_u$. Lemire et al. [41], Rohlfing [15] and Izuha and Yamanouchi [32] have analyzed it. Measurements have been made for vibrational levels up to v_1=8, v_2=37, v_3=4 [13]. In spectra with complicated structure, which may result from a strong Q-branch in Π_u-Σ_g^+ transition, the lifetime is shorter, 350 ns, than for the other (Σ_u^+ - Σ_g^+ transitions without Q-branch), 700 ns. Rohlfing got LIF in the wavelength interval 274-307 nm [32].

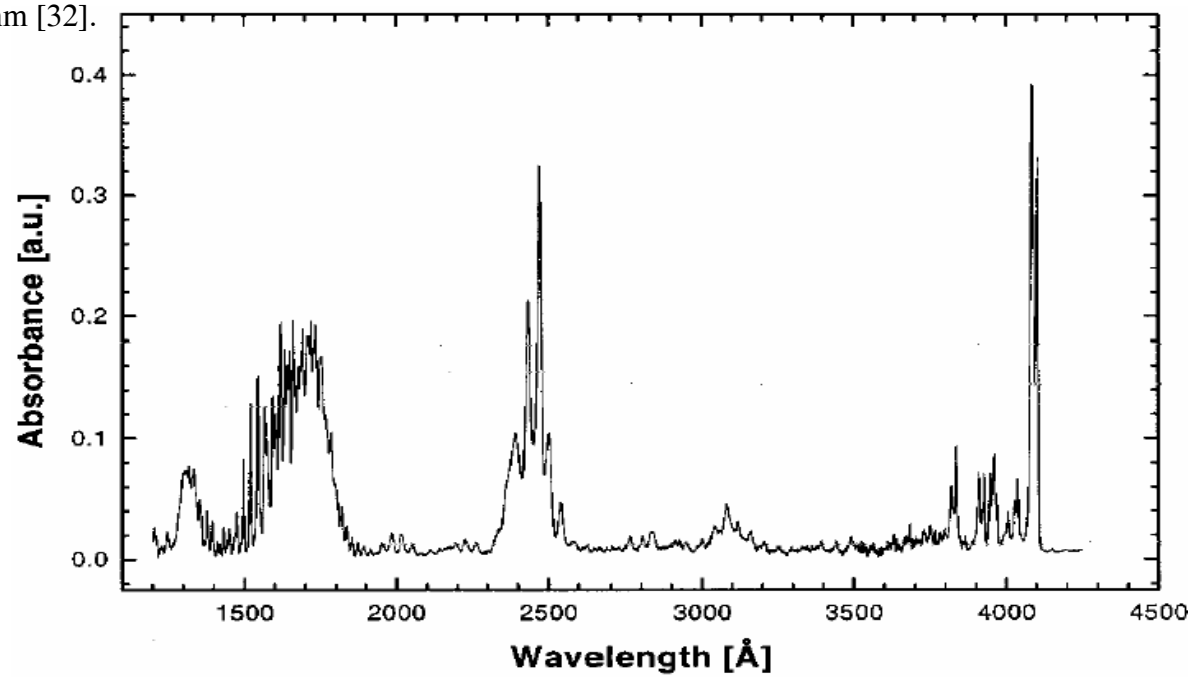

Figure 4. The lower part of the C_3 spectrum taken by Monninger et al. The peaks around 250 nm and 310 nm are not from C_3 [40].

3. Laser spectroscopy

3.1. Laser-induced Fluorescence (LIF)

Laser-induced fluorescence is fluorescence induced by laser radiation. This means that the laser excites the atom or molecule, which sends out radiation when it deexcites. In the time interval between the excitation and deexcitation non-radiative processes can occur which may have the effect that new states are populated. Since many different states are populated the fluorescence can take place on several wavelengths and it is possible to observe a spectrum.

Since we can choose both the wavelength with which we excite the molecule and the one that we observe, this makes an excellent choice to study atoms and smaller molecules. In an excited molecule many processes can take place. An electron can be excited in one way, by absorbing a photon, but it can be deexcited in several ways. It can spontaneously emit a photon, it can be stimulated to emit a photon, it can be quenched, it can be photoionized and predissociated. Luckily the two latter cases can usually be neglected. If we put up the population equation for the two levels we get:

$$\frac{dN_1}{dt} = -N_1 b_{12} + N_2 (b_{21} + A_{21} + Q_{21}) \tag{3.1}$$

$$\frac{dN_2}{dt} = N_1 b_{12} - N_2 (b_{21} + A_{21} + Q_{21}) \tag{3.2}$$

$N_{1,2}$ stands for the number of electrons in each state, b_{12} and b_{21} are the rate constants for absorption and stimulated emission**,** A_{21} is the spontaneous emission constant, Q_{21} is the quenching constant. Since it is assumed that no molecules leave the system we can set:

$$\frac{dN_1}{dt} + \frac{dN_2}{dt} = 0 \tag{3.3}$$

Now, we are only interested in the fluorescence, which is N_2A_{21}. To simplify the expressions we introduce a new variable r, as:

$$r=b_{12}+b_{21}+A_{21}+Q_{21} \tag{3.4}$$

Since A_{21} is a constant we only need to calculate N_2, which can be done by solving eq. 3.3:

$$N_2 = \frac{b_{12} N_1^0}{r}(1 - e^{-rt}) \tag{3.5}$$

where N_1^0 is the initial population in N_1. As we can see this means that after some time N_2 would reach a steady state where N_2 can be expressed as:

$$N_2 = \frac{b_{12} N_1^0}{r} \tag{3.6}$$

Reinserting r in the expression gives

$$N_2 = \frac{b_{12}N_1^0}{b_{12}+b_{21}+A_{21}+Q_{21}} = N_1^0 \frac{b_{12}}{b_{12}+b_{21}} \frac{b_{12}+b_{21}}{b_{12}+b_{21}+A_{21}+Q_{21}}$$
$$= N_1^0 \frac{B_{12}}{B_{12}+B_{21}} \frac{1}{1+\frac{A_{21}+Q_{21}}{b_{12}+b_{21}}} = N_1^0 \frac{B_{12}}{B_{12}+B_{21}} \frac{1}{1+\frac{I_{sat}^v}{I_v}} \quad (3.7)$$

Subsequently the irradiance, caused by fluorescence, can be calculated to be:

$$F == h\upsilon \frac{\Omega}{4\pi} lAN_1^0 \frac{B_{12}}{B_{12}+B_{21}} \frac{1}{1+\frac{I_{sat}^v}{I_v}} \quad (3.8)$$

In order to simplify we look at the two cases when the incoming irradiance is much less or much more than what is needed to saturate the transition. In the **linear regime** (I_v « I^v_{sat}) the transitions that are not directly dependent on the fluency dominates and the fluorescence becomes:

$$F == h\upsilon \frac{\Omega}{4\pi} lAN_1^0 \frac{B_{12}}{B_{12}+B_{21}} \frac{1}{\frac{I_{sat}^v}{I_v}} = h\upsilon \frac{\Omega}{4\pi} lAN_1^0 \frac{B_{12}}{B_{12}+B_{21}} \frac{I_v}{I_{sat}^v} \quad (3.9)$$
$$= h\upsilon \frac{\Omega}{4\pi} lAN_1^0 \frac{B_{12}}{B_{12}+B_{21}} \frac{B_{12}+B_{21}}{A_{21}+Q_{21}} = h\upsilon \frac{\Omega}{4\pi} lAN_1^0 \frac{B_{12}}{A_{21}+Q_{21}}$$

In this case it is obvious that we need to know the molecular parameters B_{12}, A_{21} and Q_{21} representing absorption, spontaneous emission and quenching. Both absorption and spontaneous emission is independent of the environment and can therefore simply be measured and tabulated. The quenching, which is a general name for the non-radiative processes exciting or deexciting states, cannot easily be measured and tabulated. Since we usually do not have the quenching constant we cannot do quantitative measurements in the linear regime. In the **saturated regime** (I_v » I^v_{sat}) the transitions that are directly dependent on the fluency dominates and the fluorescence becomes

$$F == h\upsilon \frac{\Omega}{4\pi} lAN_1^0 \frac{B_{12}}{B_{12}+B_{21}} \frac{1}{1+\frac{I_{sat}^v}{I_v}} \quad (3.10)$$

$$F == h\upsilon \frac{\Omega}{4\pi} lAN_1^0 \frac{B_{12}}{B_{12}+B_{21}} \frac{1}{1} = h\upsilon \frac{\Omega}{4\pi} lAN_1^0 \frac{B_{12}}{B_{12}+B_{21}} \quad (3.11)$$

As seen there is no longer any need to know the quenching constant, only the constants for absorption and stimulated emission, both easily measured. The reason we only need to know the absorption and stimulated emission is that they now are much larger than the quenching.

The problem with saturated LIF is that because of the temporal and spatial shape of the beam it is difficult to get rid of unsaturated areas. These unsaturated areas will then interfere with the measurements since the fluorescence in these areas still are dependent on the quenching.

In order to get quantitative data we are not bound to the saturated region. Since we could neglect the quenching if another process is much larger, it is possible to introduce a much

larger loss. In this case we can neglect the quenching and do instead use this new loss in our approximations. If this loss is well quantified we can get quantitative data. This is the case for **predissociative LIF** and **photoionization controlled-loss spectroscopy**:

In *predissociative* LIF (LIPF) we overcome the unknown loss caused by quenching by an even larger, but known, loss due to predissociation. The predissociation is an intrinsic molecular property and cannot be changed, but we can find the electronic state with the best predissociation rate for the intended purpose. However, not too surprisingly, the efficiency of these processes is low. In *photoionization* controlled-loss spectroscopy (PICLS) we also introduce a large loss, although now it is due to photoionization. In difference to LIPF we could in this case control the loss.

The loss is induced by a second laser and is expressed as:

$$W_{2i} = \frac{\sigma_{2i} I_i}{h\omega_i} \tag{3.12}$$

where W is the photoionization rate, σ_{2i} is the photoionization cross section for level 2, I is the intensity of the laser beam and ω the frequency. The index i indicates that it is the incoming beam we are interested in. This loss decrease, as with LIPF, the detection efficiency.

In air at room temperature, radiation with wavelength less than 190 nm will not penetrate. In hotter environments this may be the case up to 250 nm. This is a result of that the common gases in air, N_2, O_2, CO_2, have high absorption in this part of the spectrum. Sadly, this is also the case for other interesting species, which therefore cannot be measured with ordinary LIF. In order to circumvent this an approach called **two-photon excitation** can sometimes be used. In this case instead of one photon we have two photons involved when exciting from one state to another. Generally the absorption cross section is much lower than for the one photon case. It does also scale as I^2 in relation to the intensity of the beam.

Another way to handle the quenching is to measure it. From equation 2.5 we have the dependence of fluorescence with time. For large values of *rt* the parenthesis will be equal to one, but if the product is low enough a dependence of time could be seen. Therefore, if it is possible to arrange measurements with a small time interval, it is possible to calculate *rt* and from that *r*. Since all other constants are known it is now simple to calculate Q_{21}, the quenching rate constant.

In imaging applications two-dimensional LIF (2D-LIF) is used. In this case filters are used to select a region of the spectrum, which is well fitted to observe the selected atom or molecule. Important properties for this part of the spectrum are that the partial fraction that is measured should be independent of temperature and that the region selected should contain no other species, which interferes [42].

3.2. Laser-induced Incandescence (LII)

Laser-induced Incandescence (LII) is blackbody radiation from soot particles that have been heated by laser radiation. Since heating is necessary in order to vaporize soot there will always be LII in such cases. The LII could be used as a method to monitor the amount of soot. If this is not the case it will be a background. Since it spans the entire spectrum it is sometimes difficult to get rid off the spectral contribution from LII. What could be done to minimize the effect is to use an interference filter that match the transition of interest as good as possible. Since LII is a process that involves heating and cooling it is relatively slow. The LII-signal has a temporal length in the range up to 1 μs.

4. Experimental Setup

The experimental setup used is shown in Figure 5. The laser used was a Nd:YAG-laser with an OPO connected to it. Two laser beams were used. First a vaporization beam with a wavelength of 355 nm, which was used to vaporize the soot in order to create C_3. The pulse energy in this beam could be adjusted from 0 up to 15/50 mJ, the latter depending on the conditions of the laser, with help of a beam attenuator. The second beam, which was monitored by the OPO, was the excitation beam. This beam had in general a wavelength close to the ground transition of C_3, 405 nm; the pulse energy in this beam was about 2-3 mJ. In some cases other transitions were used to get the fluorescence in the main transition.

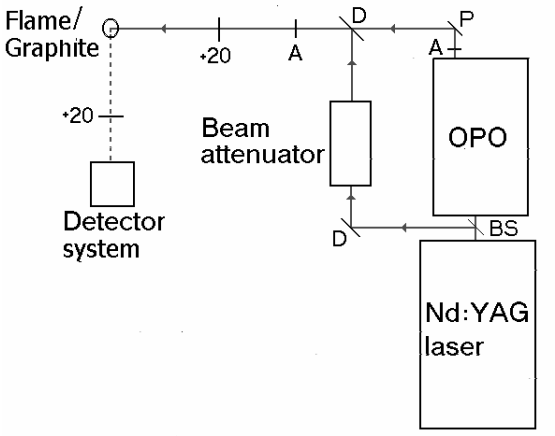

Figure 5. The Experimental Setup used. In experiments with graphite the burner is replaced with a graphite rod. In excitation scans the detector consists of a photomultiplicator with an interference filter. When taking LIF-spectra the detection system consists of a spectrometer, a CCD-camera and a short- or long-pass filter.

In the excitation scans an interference filter was used. Both 420 and 430 nm interference filters, with a bandwidth of 10 nm, a max transmission of 50 percent and with blocking OD 4, was used. In the generation of LIF-spectra a 420 nm long-pass filter was used when the excitation wavelength was around 405 nm, while a 420 nm short-pass filter was used when the excitation wavelength was 426.4 or 431.4 nm. Spectrally pure (< 6 ppm ash) graphite rods were used for investigation on graphite.

When excitation scans were recorded a photomultiplicator connected to a boxcar integrator was used. An oscilloscope showed the temporal profile of the signal. Delay lines were first used for the vaporization beam to decrease the time separation between the pulses to 5 ns. When fluorescence spectra were taken the same setup was used except that the photomultiplicator and the interference filters were replaced by a spectrometer with a CCD-camera connected to it, and a 420 nm long-pass filter.

Unless stated otherwise the gate interval, used by the detector, was 10 nanoseconds and centered on the excitation beam signal. In some cases a photodiode was used to monitor the energy fluctuations in the excitation beam.

4.1. Nd:YAG laser and Optical Parametric Oscillator (OPO)

In these experiments a Nd:YAG laser has been used. Onto this laser an Optical Parametric Oscillator (OPO) was coupled. With help of the latter we could adjust the lasing wavelength to the one preferred. The **Nd:YAG laser** is one of the most common laser types and is used both in industrial processes and in laboratory work. The lasing wavelength is 1 064 nm, but for many purposes it is frequency doubled to 532 nm. Also third respectively fourth harmonic beams are used frequently, giving the wavelengths 355 and 266 nm. The laser is a solid-state laser and can run both in continuous wave and pulsed mode; in the later case Q-switching is used. When used in pulsed mode the pulse rate is commonly 10 Hz. The pumping can be done either by a flash lamp or by a semiconductor laser.

In the investigations we needed laser light with a wavelength of 405 nm. In order to get this wavelength an **OPO** is used. As in many applications where the wavelength cannot be easily reached with a commonly available laser an OPO can be of great use. With the OPO it is possible to change the wavelength to the preferred region and still have a narrow line width, which in many applications makes it preferable in comparison with dye lasers. Dye lasers can be tuned within a selected wavelength range but has a broader line shape.

In order for the Parametric Oscillation to take place we need, except for the incoming ω_3 beam also an, although weak beam ω_1. Together theses beams form a third beam, the signal beam ω_2. For the conversion we have the relationship given in eq. 4.1, since the energy must be conserved inside the system:

$$\hbar\omega_3 = \hbar\omega_1 + \hbar\omega_2 \tag{4.1}$$

As in second harmonic generation the new wave will gain in strength when it passes through the medium while the source wave will lose strength. In many senses its behavior is laser-like since we have some kind of "*active medium*" while letting light out of a partially transparent mirror. The mirrors have high reflectivity (R_1=1, R_2 ~1) for at least ω_2 (singly resonant oscillator), but often also ω_1 (doubly resonant oscillator). In the first case the threshold pump power is higher since more of the "pump beams" leaks out [42, 43].

4.2. The Photomultiplicator

When a photon hits the cathode, electrons are released. The release of electrons depends on the work function of the cathode material. Between the cathode and the anode there is a number of dynodes. Between each of these dynodes we have a difference in electric potential. Because we have this difference the electrons gain energy when accelerated towards the next dynode. When an electron hits the dynode it will therefore have an energy that is many times larger than when it was released. Because of the high energy it can release a large number of electrons when it hits the dynode. The process will then repeat itself as these electrons accelerate towards the next dynode.

Photomultiplicators are very sensitive and can under the right conditions count single photons. However there is noise, mostly from three sources of noise:

* **Shot noise**
* **Multiplication noise**
* **Thermal noise**

In the photomultiplicator a dark current is created from spontaneous emission of electrons due to their random motion. Together with an uncertainty in the converting from photons to electrons, which is due to the quantization of the current, this creates a *shot noise*. The shot noise is Poisson-distributed. When an electron hits a dynode the number of released electrons could vary, this variation is called *multiplication noise*. The *thermal noise* is a result of the random motion of electrons in the resistive elements, i.e. in the electronics after the signal is amplified [42, 44].

4.3. The Boxcar Integrator

The photomultiplicator creates an electronic signal from the detection of photons, but to make it useful some treatment is needed. The fluorescence signal is in general in the nanosecond timescale. With no further treatment it would drown in background noise. To select the fluorescence signal gating is used. The boxcar gets a signal from the laser when it should start receiving the photomultiplicator signal and do then measure for a given time interval.

The boxcar can be used in three regimes. In the linear averaging mode the signal will be the sum of the last signals, the integration is done analogically in the electronics. For the exponential mode the same is true with the difference that later pulses have an exponentially higher weight, still by analogical integration. In those modes the noise will start averaging down to zero the more pulses are collected, thereby improving the signal to noise ratio. In sample and hold mode each pulse is sampled individually and the data analysis could be done completely separate [42].

4.4. The CCD-camera

The CCD-camera (CCD is a abbreviation for Charged-Coupled Devices) is in principle an array of photosensitive semiconductors. There are no charges in the depletion region of a semiconductor. If a photon hits this area an electron-hole pair is created, which will introduce a current in the circuit. The quantum efficiency is in general good, usually over 50 %. Each pixel work as a potential well and therefore the charges could be stored in the CCD over long periods, which is useful for long measurements.

The large numbers of pixels need to be read out limit the speed of the camera, which could limit the usability of the camera. The thermal noise is another important problem for CCD-cameras. Electrons have a spontaneous motion that is proportional to the temperature. In order to reduce this noise the camera needs to be cooled [42, 44]. In our case water was used as coolant.

4.5. The Spectrometer

To separate light/radiation with different wavelengths, spectrometers are used. Nowadays almost all spectrometers use gratings, which are more accurate than prisms, which were used earlier. The grating consists of a repetitive array of element that produce changes in the phase or amplitude of the incoming light. These elements will cause interference phenomena. For the grating we have:

$$d(\sin\theta_m - \sin\theta_i) = m\lambda \qquad (4.2)$$

where d is the size of the individual grating, θ_m and θ_i the angle of the outgoing and incoming light, m the order of the constructive interference and λ the wavelength of the light, as seen in Figure 6. Therefore, when the wavelength is changed there will be a change in the place where we have constructive interference. From eq. 4.2 we get the wavelength as

$$\lambda = \frac{d(\sin\theta_m - \sin\theta_i)}{m} \qquad (4.3)$$

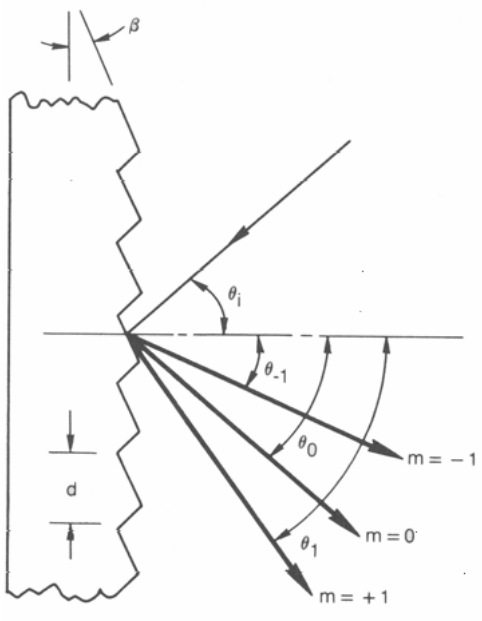

Figure 6. Principal sketch of an incoming beam hitting a grating and the zero and first order constructive interferences [42].

From eq. 4.3 it is seen that an incoming wave will have constructive interference for several wavelengths, with different values of m. These phenomena are called ghost images and are a problem for all non-holographic gratings.

The resolution of the spectrometer is dependent on the size of the entrance (and exit) slit (s), the grating used, and the focal length (f)

$$\frac{d\lambda}{ds} = \left(f \frac{d\theta}{d\lambda} \right)^{-1} \tag{4.4}$$

5. Measurements and Results

Investigations have been made on graphite and in a welding torch. In the experiments the excitation wavelength, the energy in the vaporization beam, the height in flame and the flame composition have been changed between the experiments. In a few cases the time difference between the vaporization and excitation beam has been lowered. The primary goal of the measurements was to get an observable signal from C_3 and after that to find its dependence on changing conditions. Since no definite C_3 signal was found only the first part was done.
In all spectra from graphite, reflection of the laser beam can be seen and in all spectra from the welding torch the laser beam is Rayleighscattered. In both cases this gives as result a signal of the laser beam that show up in the LIF-spectra.

5.1. Graphite

Graphite is pure carbon in a crystal structure with strong bonding in the plane, which has a hexagonal structure, and weak bonding between the planes. This basic structure of graphite corresponds quite well to the structure of soot, where graphite layers are found, but with lots of dislocations. Soot contains 90 % carbon and 10 % hydrogen, when the soot is formed the hydrogen content is higher than later in the process. In graphite it should in principle be easier to create C_3 than in flames since there is a much higher concentration of carbon, which is the source of C_3-formation. Graphite has been a common source of C_3 in high-resolution spectroscopy.

The use of graphite caused several problems, which did not exist in the flame. The most severe was the problem that beams easily were so concentrated that they burned hole in the graphite. No fluorescent light could then hit the detector because it was hidden by graphite. Measurements have been made both with focused and unfocused beams.

5.1.1. Excitation scan

In order to find the exact spectral position of transitions at a given temperature excitation scans were taken. The oscilloscope showed that both the excitation beam and the vaporization beam contributed to the signal. Several excitation scans in the range 398 to 410 nm were taken. The energy in the vaporization beam was changed. The experimental setup was also changed as unwanted disturbances and errors were detected. The changes were in general to add and move black plates in order to hide and remove reflexes. Reflection seemed to be a major problem and in order to decrease it, the 420 nm interference filter used were replaced with a 430 nm interference filter. The reason for this change was that the wing of the laser profile becomes weaker further away from its peak, Rayleighscattered light will therefore not interfere the measurement in the same way with the 430 nm interference filter. The change did however not lead to any qualitative change.

The intensity of the focused vaporization beam was high, higher than 100 mJ/mm^2, this had as effect that a hole was burnt. This energy is much higher than the energy needed to vaporize graphite. The intensity needed to vaporize graphite is less than 3 mJ/mm^2 [13]. The vaporization beam gives unfocused an intensity of about 1 mJ/mm^2 for the energies used in the vaporization beam. It was therefore possible that this energy might not vaporize the graphite, however to circumvent the high intensity problems it would have been needed to continuously rotate the graphite rod, which was not practically possible. To use an unfocused beam was therefore preferable, although not optimal.

When the beam was unfocused it happened under some short periods that the signal became much stronger than otherwise, as could be seen in the region 402-403 nm in Figure 7. It then

suddenly fell back to the normal level. From scan to scan the shape of the spectrum was changed (see Figure 7-9). The signal was proportional to the energy in the excitation beam, but independent of the energy in the vaporization beam.

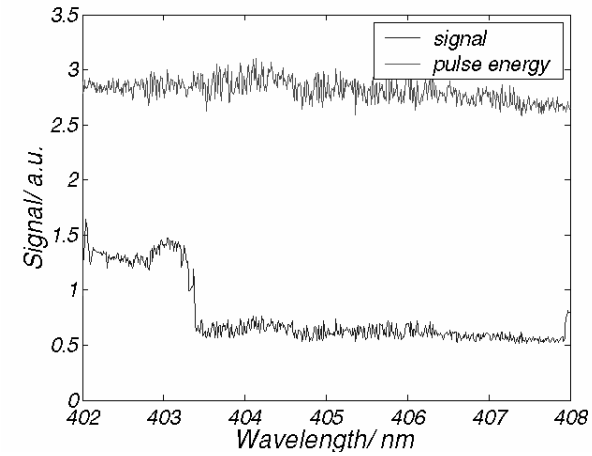

Figure 7. Excitation scan on graphite with about 20 mJ in the vaporization beam. The photomultiplicator is on 648 V. No focusing lens is used.

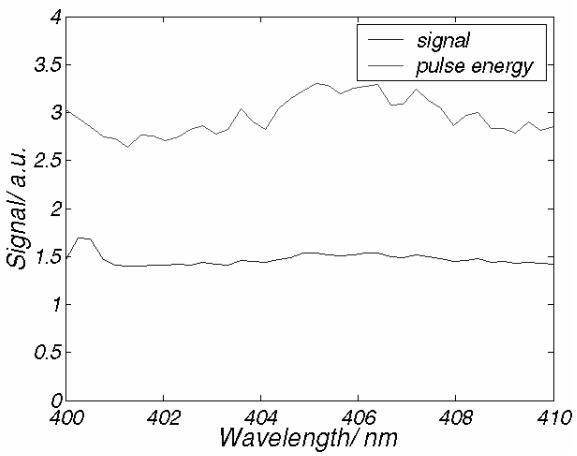

Figure 8. Excitation scan on graphite with about 20 mJ in the vaporization beam. The photomulticator is on 567 V. No focusing lens is used.

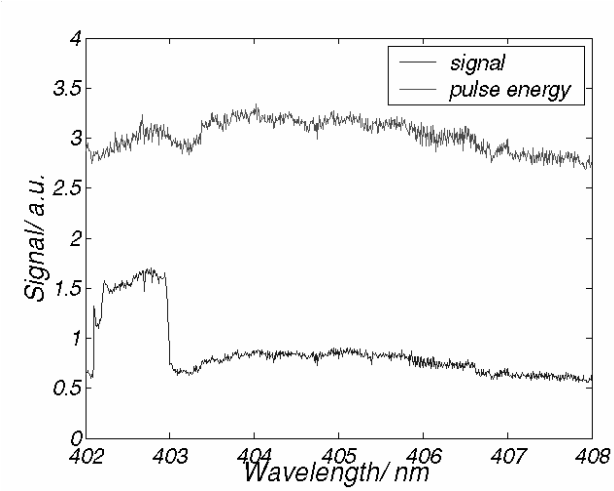

Figure 9. Excitation scan on graphite with about 20 mJ in the vaporization beam. The photomultiplicator is on 648 V. No focusing lens is used. The signal has a length of around 27 ns.

5.1.2. LIF-spectra

The excitation scans give information of the total fluorescence when atoms and molecules are excited at different wavelengths. But, it only tells us how much the total fluorescence is, not what it looks like. In order to see if the signal is from LII, from C_3 or from another molecule LIF-spectra are useful.

For low energies in the vaporization beam, and excitation wavelengths around 405 nm the LIF-spectra on graphite show a small peak around 440 nm, as shown in Figure 10. LIF-spectra were also taken with changing wavelength of the excitation beam over a wider interval. It was found that the wavelength of the peak in these cases was dependent on the excitation wavelength. The shorter the excitation wavelength, the longer was the wavelength of the peak. The increasing frequency in the excitation beam was shown to match the decreasing frequency in the signal well, as seen in Table 4. The total wave number for the excitation beam and the signal is between 47 700 cm^{-1} and 47 850 cm^{-1}.

Table 4. Excitation wavelength and signal wavelength from LIF-spectra on graphite. No energy in the vaporization beam.

Excitation	Signal
395 nm	445,15 nm
396 nm	443,47 nm
397 nm	443,67 nm
398 nm	441,00 nm
399 nm	439,51 nm
400 nm	439,31 nm
401 nm	436,94 nm
402 nm	436,44 nm
403 nm	435,45 nm
404 nm	433,37 nm

When the energy in the vaporization beam was increased it was suppressed by a larger and broader signal as seen in Figure 10. The signal has its peak around 450 nm.

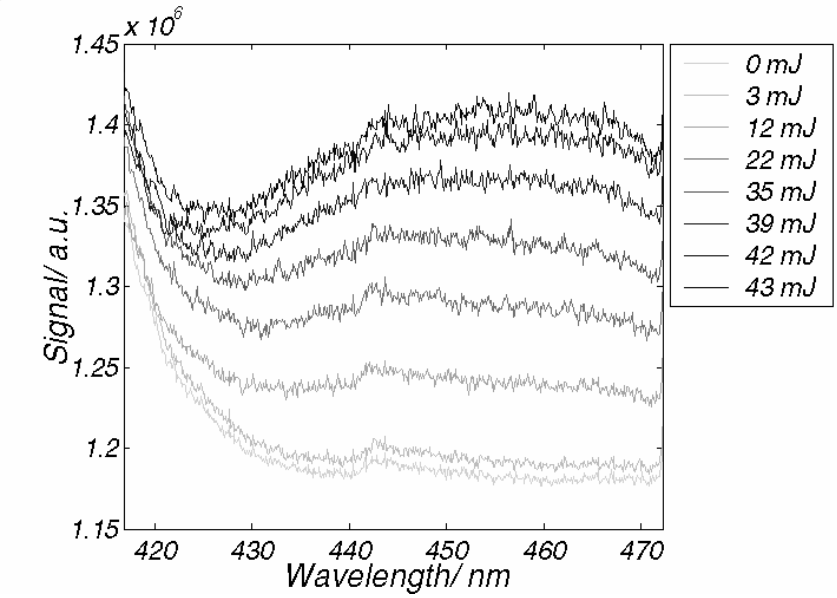

Figure 10. LIF-scan on graphite, with varying energy in the vaporization beam. The excitation beam is on.

5.2. Welding torch

The advantage of using a welding torch is that it often is easier to get a signal in a welding torch than in other flames. In difference to vaporization of graphite we have soot, not graphite vapor to measure on. We are therefore closer to real measurements. On the negative side it is not possible to control the flows with good quantitative accuracy in a welding torch

5.2.1. Excitation scan

The excitation scans were taken with different pulse energies in the vaporization beam and with the excitation wavelength at 405.0 nm. The oscilloscope showed that the signal has a temporal length of about 200 ns and the strength of the signal increased when the energy in

the vaporization beam was increased. Excitation scans did not show peaks corresponding to C_3. Instead the spectrum changed from scan to scan, as could be seen in Figures 11 and 12.

Excitation scans were taken with both 5 and 10 ns time separation between the vaporization beam and the excitation beam. The only difference was an observable time separation between the signal from the vaporization beam and the excitation beam.

When the energy in the vaporization beam was changed, the signal strength increased proportional to the energy in the vaporization beam. The curves, seen in Figures 13 and 14, fit each other well, with correlation coefficient, $\mathbf{R^2 \approx 0.97}$, where $R^2=1$ indicates that the two parameters are directly proportional to each other, while $R^2=0$ indicates that there is no relation between the two parameters.

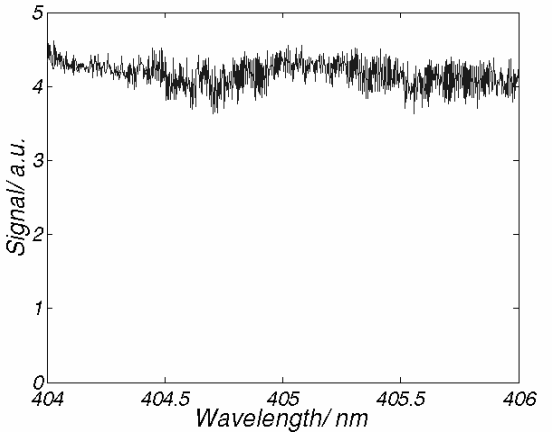

Figure 11. Excitation scan in flame with 10 mJ energy in the vaporization beam.

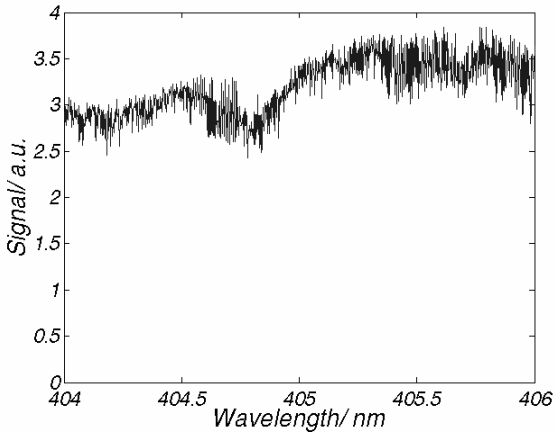

Figure 12. Excitation scan in flame. No energy in the vaporization beam.

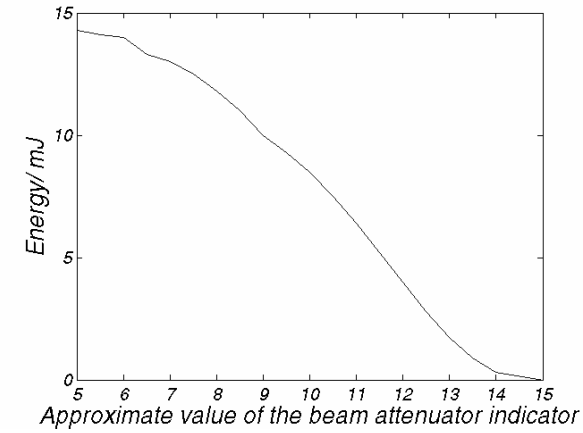

Figure 13. The output energy from the beam attenuator as a function of the value of the beam attenuator indicator

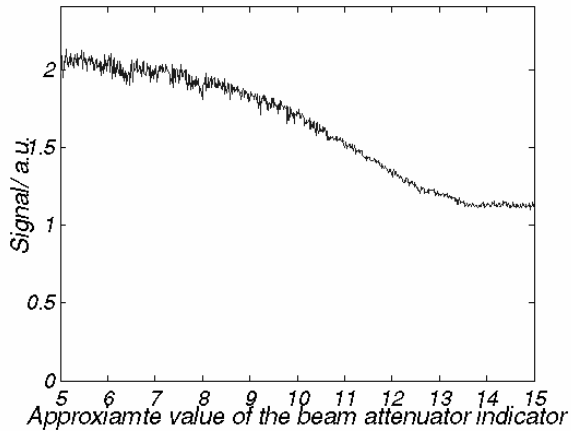

Figure 14. Excitation scan on graphite. The beam attenuator is changed continuously and the signal measured.

5.2.2. Fluorescence Spectra

In the welding torch a lot of molecules exist, therefore it is important to not only take excitation scans but also fluorescence spectra in order to be sure of what is measured.

The first spectra were taken under *incorrect alignment*. The excitation beam and the vaporization beam did not focus on the same place and therefore no LIF from vaporized soot fragments could be expected. To gain more information spectra were taken at different

heights since the abundance of soot and other particles change due to the chemical reactions in the flame. In the pure acetylene flame, using a pulse energy in the vaporization beam of approximately 13 mJ, a LII-type signal could be seen at first, together with, in some cases, a peak around 470 nm, see Figure 15. However, under the same conditions, but with oxygen added, a signal was observed with a wavelength around 431 nm, shown in Figure 16. Changing the energy in the vaporization beam did not change the signal strength. As a test for what could cause the signal a pseudo-excitation scan was taken. The scan consisted of LIF-spectra taken with an interval of 0.2 nm in the range between 395 and 410 nm. The total fluorescence in the region 429 nm to 434 nm was calculated. The scan showed no sharp structure, as can be seen in Figure 17.

When the ***setup was correctly aligned*** new LIF-spectra were taken. The LIF-spectra, when only having the excitation beam on, showed LII and some small peaks around 435 nm and 470 nm, as seen in Figure 18. When the vaporization beam was turned on with energy around 8 mJ the contours around 435 nm and 470 nm showed more strongly, see Figure 19.

Excitation with the wavelengths **426.4** and **431.4 nm** was also done. These wavelengths corresponds to excitation of the anti-stretch vibration respectively the A (0,0,1)-X (0,0,1) transition. Excitation with 426.4 nm only gives the laser profile from Rayleighscattering as result; while in the case of 431.4 nm there also exists a structure around 410 nm, seen in Figure 20. The later experiments were repeated with McKenna-burner with the same result.

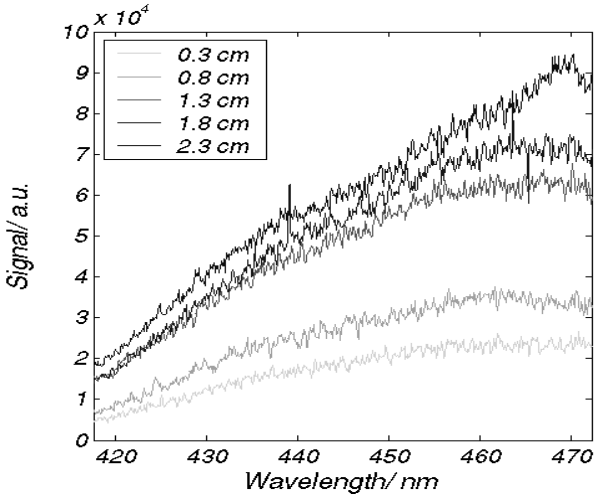

Figure 15. LIF-spectrum for a pure acetylene flame, with excitation wavelength 405.0 nm and a pulse energy of 13 mJ in the vaporization beam.

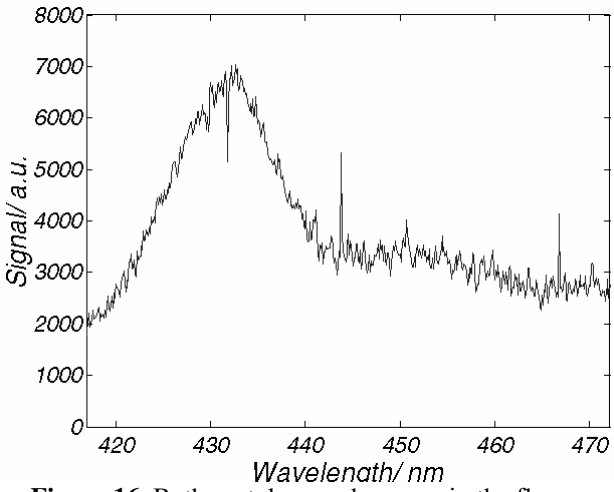

Figure 16. Both acetylene and oxygen in the flame, averaging from measurements on different heights. The difference between the signal with and without the vaporization beam is taken.

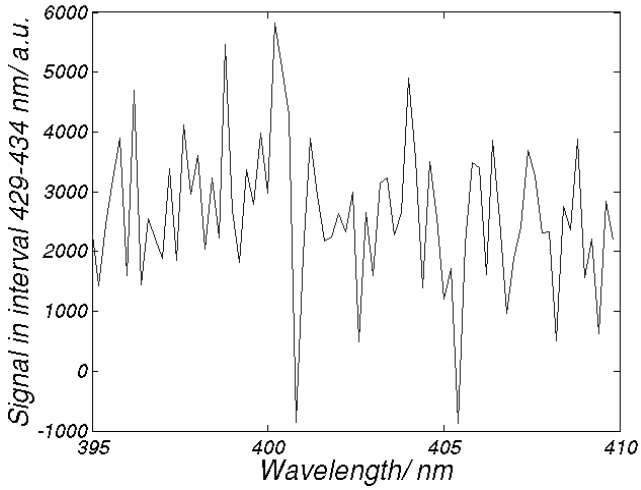

Figure 17. Pseudoexcitationscan using the LIF-spectra in the region 429-434 nm. No vaporization beam used.

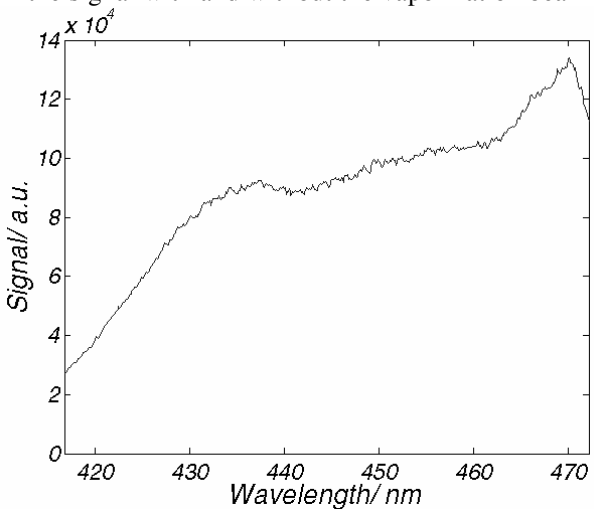

Figure 18. LIF-spectrum for a pure acetylene flame with excitation wavelength 405 nm and pulse energy of 13 mJ. Spectra are taken on heights between 0.3 cm and 2.3 cm with An interval of in average 0.25 cm. Those specta are averaged.

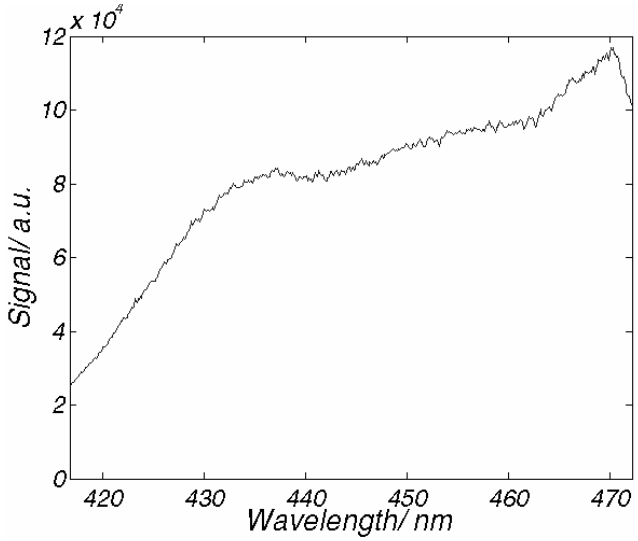

Figure 19. LIF-spectrum for a pure acetylene flame with excitation wavelength 405 nm and a pulse energy of 8 mJ. Spectra are taken on heights between 0.3 cm and 2.3 cm with an interval of in average 0.25 cm. Those spectra are averaged.

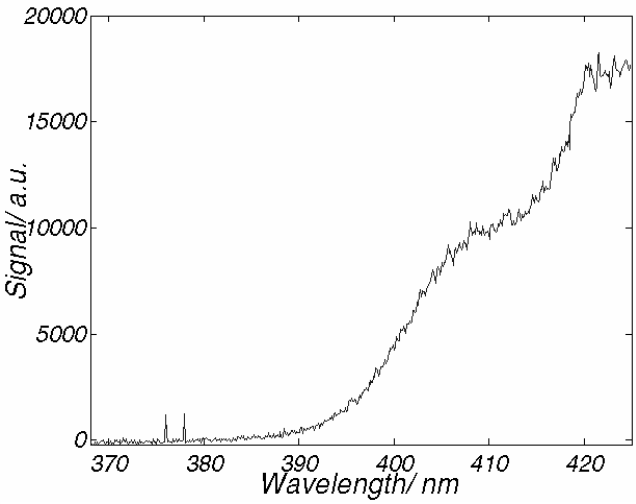

Figure 20. LIF-spectrum for a pure acetylene flame with excitation wavelength 431.4 nm taken at height 1.0 cm. The pulse energy has been varying from 6.5 to 15 mJ and those spectra are averaged.

5.3. Possible sources of errors

The measurements using excitation scans are qualitative rather than quantitative. One problem was to establish the wavelength scale of the scan accurately. The reason was that there was no possibility to start the laser scan and the boxcar integrator at the same time. The scans given could therefore differ about one or two tenths of a nanometer. The same is true for other measurements, as when the energy in the vaporization beam is changed, even in this case it is done manually and therefore with larger sources of error.

The LIF-spectra, on the other hand, are in general quite well quantified. The excitation wavelength is correct within the errors of the Laser/OPO-system. However, the fluorescence is in general very weak and in order to get an observable signal averaging of over some hundred shots is needed. The excitation scan signal is also weak and high voltages on the photomultiplicator are needed. In order to minimize the errors, LIF-spectra were taken with the laser blocked between the measurements. In this way potential background from the room light and excitation from the flame could be subtracted.

The laser has both long-term variations and shot-to-shot variations. The variations in pulse power from shot to shot could vary as much as 50 %. The long-term variations, which could take place over several minutes, were in many ways more severe since they were realized only at the end of the experiments. The long-term variations seemed to be about 20 %. Finally the output energy of the laser system decreased with time as the experiments were made, the maximum output after the beam attenuator decreased from roughly 50 mJ to around 15 mJ.

Two different methods were used to set the gating. For the excitation scans the gate was placed with help of the oscilloscope. With help of the oscilloscope the gated interval is chosen to be around the peak of the excitation beam. In the case of the LIF-spectra it is impossible to use the oscilloscope. The gating is instead selected to be in the center of the range where signal was observed. The gating is therefore less accurate in comparison with excitation scan gating, since in this case we had no knowledge of the temporal profile of the laser beams. In the latter case we would collect more signal from the vaporization beam compared to the excitation scan, since it is the center to the entire signal that is taken, not only the signal from the excitation beam.

The spectral sensitivity, i.e. the response of the detector on light with different wavelength, is not measured. This introduces an uncertainty in the interpretation of the spectral data. The filters used, which transmission depends on the wavelength, introduce another uncertainty. The transmission is only known for a few wavelengths and from these values the transmission profile has to be interpolated. Except for the errors in measuring the transmission this do introduce errors in the fit of these values to a curve.

6. Discussion

6.1. Earlier Measurements

Earlier measurements has been done in 1996 by Raiche and Jeffries [5], in 1997 by Luque et al. [6], in 2000 Takizawa et al. [7] and in 2002 by Sasaki et al. [8]. The original goal of Raiche and Jeffries was to measure CH, but because their spectra were interfered by C_3 it got their attention. In their paper from 1996, C_3 was excited at (v_1, v_2, v_3=0,0,0) and fluorescence measured at (1,0,0). In the paper from 1997 the opposite procedure was used, exciting at (1,0,0) and measuring at the fluorescence back to (0,0,0). In the latter case LIF-signals could also be obtained from C_2 (d-a), CH (A-X) and CH (B-X). In the experiment by Takizawa et al., C_3 was excited at 405.13 nm and fluorescence was observed at 407.3 nm. This fluorescence resulted from excitation at (0,0,0) and fluorescence back to (0,2,0). The relative density was then measured from this peak.

When using high laser irradiance (40 $\mu J/mm^2$), the spectrum disappeared in a continuous baseline signal resulting from hot band excitations [5]. Quenching shortened the excited state lifetime from 200 ns to 22 ns with a difference between individual energy levels being less than 5 % [5]. Due to the complicated spectrum it was difficult to make quantitative measurements. In ref. 5, theoretical summation of the J-states from 0 to 52 in the R-branch for the (0,0,0)-(0,0,0) transitions was used, in ref. 6, cross section measurements made by Cooper and Jones [45] was used instead.

In order to get an understanding of the processes behind the creation of fullerenes and nanotubes, Sasaki et al. measured the distribution of C_2 and C_3 in laser-ablated carbon plumes by LIF. The process took place at low pressures. They observed self-emission on the same wavelength as the fluorescence was measured.

6.2. Graphite

The use of graphite showed mainly reflectance, though some odd behavior could be found. No signal could be assigned as originating from C_3. This was unexpected since graphite has been used as a C_3-source in high-resolution spectroscopy of C_3. This might be a result of quenching since these experiments were performed with high temperature and atmospheric pressure, in comparison with the spectroscopic studies that generally were performed with low temperature and at low pressure, it may also be a result of too low vaporization intensity.

When excitations scans were recorded it happened that under some short periods the signal became much stronger than otherwise. This might be a result of vaporization of irregularities in the graphite. In some cases this vaporization may have created more areas that reflect the laser beam directly towards the detector and caused the signal to become stronger. The reason cannot be varying pulse energy since the signal otherwise is proportional to the beam energy. Since the signal is independent of wavelength, it is not LIF. Since the signal strength still is proportional to the energy in the excitation beam, but independent of the energy in the vaporization beam, this indicates that we still see reflection and nothing else.

Reflection is also seen in the LIF-spectra. Since the LIF-spectra are integrations of hundreds of shots it is not possible to get spectral information of this signal, since the long shoot series makes it impossible to see those abrupt changes. When the excitation wavelength was changed over a wider interval it was shown that the increasing frequency in the excitation beam matched the decreasing frequency in the detected signal well. This makes it probable that the peak has its origin from phenomena in the OPO. Since the signal was much weaker

than the reflection of the main laser pulse it was not possible to see its temporal position on the oscilloscope.

The broad peak, shown in Figure 10, is difficult to explain. It might be Poly Aromatic Hydrocarbons (PAH) from vaporized graphite since it is very broad. PAH consists of a varying number of benzene rings and has a very broad spectrum. Since no C_2 is seen this do pose the problem of explaining why PAH should be created, but not C_2. One possible reason might be that it is the weak bonds in graphite that is first broken when graphite is vaporized. In this case graphite would be vaporized plane by plane, which would increase the probability that PAH is created. Even though it at a first look might look like LII it is almost definitely not. Since it peaks around 450 nm it would indicate a temperature of 6 400 K, the curve should also be more flat in that case. Since the spectral sensitivity is not measured it is possible that the peak is mal-positioned due to differing spectral response at different wavelengths for the CCD-camera. However, this would probably not change the peak position more than a few nanometers.

6.3. Welding torch

In the welding torch, spectral peaks matching CH and C_2 were found as a superposition on top of LII. Since neither CH nor C_2 has an electronic transition close to the used excitation wavelength this could imply that those species are far more abundant than C_3 if C_3 would be detected.

The presence of LII could be seen in all measurements. It could be seen both in the excitation scans and in the LIF-spectra. When taking the excitation scan it could be seen with the oscilloscope that the signal had a temporal length of around 200 ns. This corresponds well to the temporal length of LII. It is, however also the time range for the used ground transition without quenching. But since we have quenching it is expected to be considerably shorter [5]. Blocking of the excitation beam also shows that the signal comes from the vaporization beam, which would be expected if it were LII. In LIF-spectra it is possible to see LII as a background in all spectra.

When the flame contains oxygen a signal with a wavelength of 431 nm is seen. It has probably its origin in the CH A-X transition. Even if the A (0,0,1)-X (0,0,1) transition of C_3 has the same transition wavelength that peak would be more narrow. The higher rotational constant for CH makes the peak broader and CH fits the spectrum, seen in Figure 16, rather well. This is not the case for the C_3 transition since the low rotational constant together with a higher rotational constant for ground level than for the excited level makes the peak very steep on the red side of the transition wavelength. CH is abundant in welding torches and it is therefore not unexpected to see it, even if the absorption is not strong at wavelengths around 405 nm. When changing the energy in the vaporization beam the signal do not change. This indicated that the molecule found was not created by vaporization of soot. This should not be the case since the alignment was not correct and therefore the excitation beam did not excite the molecules from the vaporized soot. One more indication that the source is not C_3 is the pseudo-excitation scan, which shows no clear structure. Apart from CH another possible source is PAH which has a broad spectrum. Even if those measurements were done with incorrect alignment they give important information of what kind of background that should be observed if the method worked.

When the vaporization beam is on peaks around 435 and 470 nm are observed in the acetylene flame. These peaks correspond well to the 2-0 and 2-1 transitions in the Swan bands of C_2. Since the signal strength is dependent on the energy in the vaporization beam it is probable that it is a result of vaporization of soot. Since C_2 is excited in spectral regions where the absorption is very low this indicates that the amount of C_2 under these conditions is considerable larger than the amount of C_3.

The LIF-spectra using 431.4 nm as the excitation wavelength shows except for the laser profile also a peak at around 410 nm. This is probably from the same phenomena in the OPO as for the experiments on graphite. The total wave number of the main laser beam and the small peak fit in the same range as for those experiments, 47 750-47 850 cm^{-1}. It is not caused by vaporization of soot since it is independent of energy in the vaporization beam.

All the above transitions do fit well with the result from the excitation scans since neither LII, nor LIF from CH or C_2 should change considerably in transition strength over the scanned interval.

6.4. The absence of observed C_3 signal

In the experiments no signals from C_3 were observed. The absence of observed C_3 signals could have a few possible explanations; the most probable being quenching and the broad spectrum of C_3.

Quenching will always exist as a factor limiting the lifetime of excited states. Higher temperature and pressure increase the quenching and decrease the signal strength. In the vaporized soot the temperature is about 4 500 K. The range of this decrease in this case is unknown, but in other cases it has been severe [5].

The broad spectrum of C_3 can be another explanation. Since C_3 has three atoms, while C_2 has two, there are more possible energy levels for the electrons, and the numbers of possible transitions are larger. In comparison with C_2 an excitation on a given wavelength will excite a smaller fraction of the molecules. The low bending constant also makes the C_3 spectrum broader and therefore the exciting laser beam will excite a lesser part of the population.

Another possible reason, though less probable, is that the chemistry of soot vapor might be different from the chemistry of pure graphite vapor. However, if hydrogen is available C_3 can be created from the reaction $C_2H + C \rightarrow C_3H$, where the latter spontaneously lead to creation of C_3 by the exothermic reaction $C_3H \rightarrow C_3 + H$. The hydrogen content in soot should therefore not be expected to decrease the C_3 content radically. In the same way it is possible to create C_3 through reactions between C and C_2H_2, also in this case C_3 is created in the ground state. [46]

Finally, it is possible that C_3 is created in one of the triplet states, a $^3\Pi_u$ or $b^3\Pi_g$. The lifetime for spin-forbidden decay to the ground level is 20 ms. This time is much longer than the time range of LIF-phenomena. In this case there will therefore be no electrons in the X $^1\Sigma_g^+$ or A $^1\Pi_u^+$ levels and no fluorescence will be seen. It is not necessary for C_3 to be created in those states, it could relax non-radiative to a $^3\Pi_u$ for both A $^1\Pi_u^+$ and $^1\Sigma_u$ [40]

7. Summary and Outlook

One of the major constituents in graphite vapor is C_3. Soot has many similarities with graphite such as high carbon content and similar structure, though it should be noted that there also are important differences. As a consequence of these similarities C_3 spectroscopy has been purposed as a method to measure soot concentrations. By first vaporizing soot and then taking laser-induced fluorescence (LIF) spectra it should in principle be possible to monitor the soot content. In this work the potential for C_3 spectroscopy has been investigated.

The C_3 molecule was identified in 1951. Since then numerous papers on the properties of C_3 has been written. The literature on electronic bands as well as on thermodynamical and chemical properties is examined in this work. Recent works on practical applications of C_3 spectroscopy are described. The most important combinational and perturbation effects are explained.

Laser-induced fluorescence in the form of excitation scans and fluorescence spectra have been taken in flames and on graphite. An excitation beam, with wavelength 405 nm, exciting the A-X transition, is used to detect C_3. The soot was vaporized with a vaporization beam, with energies up to 15/50 mJ, the latter depending on the conditions of the laser. In excitation scans the signal is collected with a photomultiplicator and filtered by interference filters. For the fluorescence spectra a CCD-camera is used together with short pass filter.

The use of graphite suffered from problems caused by the high laser intensity that burned hole in the graphite. Only reflectance was seen, no C_3 fluorescence. The absences of any observed signal from C_3 might depend on quenching, since it has been observed in other experiments done on vaporized graphite. The intensity used to vaporize soot may also have been to low.

In the welding torch signals from C_2 and CH were observed superimposed on LII. The C_2 fluorescence is supposed to have its origin in the vaporized soot since the signal depended on the energy in the excitation beam. CH on the contrary has its origin in the flame. As was the case for graphite C_3 was not observed.

Since C_3 was not observed in graphite neither in flame the reasons for this is of interest. One possible reason for the absence of signal from C_3 might be the quenching. The temperature in the vaporized soot is high, about 4 500 K, which favor quenching. The broader spectrum from C_3, caused by the additional atom, in relation to C_2 has as effect that the absorption in each part of the spectra is weaker and therefore decrease the fluorescence. This has effects both in the ground state and in the excited state. In the ground state it has as affect that fewer molecules are excited, since the electrons have more possible vibrational states to be in. The effect is extra strong since the bending vibration has a low bending constant and therefore is easily excited. In the excited state the additional vibrational modes lead to a broader spectrum, which decrease the fraction measured with a filter. Less probable reasons for the absence of signal might be differences in the chemistry between soot vapor and graphite vapor, or that C_3 is created in one of its triplet states.

To use longer carbon chains is probably not a useful concept since they have more complicated spectra and are less abundant. The most abundant longer carbon chains are C_5 and C_7, both are about three times less abundant than C_3 at the temperature of vaporized soot, 4500° C [14]. The newly identified $^1\Sigma_u$ electronic state has strong absorbance in the transition from the ground level, however this only changes the excitation wavelength, the same ground state is still used.

8. Acknowledgements

I want to thank my supervisor Per-Erik Bengtsson for many good ideas on how to prepare and set up the experiments, to evaluate the results, and last but not least all help with writing this document. I also want to thank Henrik Bladh and Martin Rupinski who have taught me a lot of things about how to work in the laboratory and been of great help for their knowledge of find the correct equipment and how to use it. I also want to thank them for all help when I have had any questions.

9. Symbols and Abbreviations

Abbreviations

LIF	Laser-Induced Fluorescence
LIPF	Laser-Induced Predissociative Fluorescence
OPO	Optic Parametric Oscillator
PAH	Poly Aromatic Hydrocarbon
PICLS	Photoionization controlled-loss spectroscopy

Symbols

A_{21}	the spontaneous emission constant
$\alpha_{1,2,3}$	the vibration-rotation interaction constant
$b_{12,21}$	the rate constants for absorption and stimulated emission
B_v	the rotational constant
D_v	the centrifugal distortion constant
ε	the Renner-Teller coefficient
F	the fluorescence
I	the (laser) intensity
J	the total rotational quantum number
l	the electron rotational quantum number
Λ	the total orbital angular momentum
N	the number density in each electronic state
q	the l-type splitting constant
Q	the quenching rate constant
S	the total spin quantum number
σ	the crossection (in this work the photoionization cross section)
$v_{1,2,3}$	the vibrational quantum number
W	photoionization rate
$\omega_{1,2,3}$	the vibration constant
Ω	the collection solid angle

10. References

1. Huggins, W., *Preliminary Note on the Photographic Spectrum of Comet b 1881*, Proceedings of the Royal Society of London, **33**, 1, 1881.

2. Herzberg, G., *Laboratory Production of the λ 4050 group occurring in cometary spectra; further evidence for the precence of CH_2 molecules in comets,* Astrophysical Journal, **96**, 314, 1942.

3. Herzberg, G., *Spectroscopic Studies of Molecular Structure*, Science, **177**, 123, 1972.

4. Douglas, A.E., *Laboratory Studies of the λ 4050 group of cometary spectra*, Astrophysical Journal, **114**, 466, 1951.

5. Raiche, G.A. and Jeffries, J.B., *Observation and spatial distribution of C_3 in a DC arcjet plasma during diamond deposition using laser-induced fluorescence*, Applied Physics B, **64**, 593, 1997.

6. Luque, J., Juchmann, W. and Jeffries, J.B., *Spatial density distributions of C_2, C_3, and CH radicals by laser-induced fluorescence in a diamond depositing dc-arcjet,* Journal of Applied Physics, **82**, 2072, 1997.

7. Takizawa, K., Sasaki, K. and Kadota, K., *Characteristics of C_3 radicals in high-density C_4F_8 plasmas studied by laser-induced fluorescence spectroscopy*, Journal of Applied Physics, **88**, 6201, 2000.

8. Sasaki, K., Wakasaki, T., Matsui, S. and Kadota, K., *Distributions of C_2 and C_3 radical densities in laser-ablation carbon plumes measured by laser-induced fluorescence imaging spectroscopy,* Journal of Applied Physics, **91**, 4033, 2002.

9. Weltner Jr, W. and van Zee, R, *Carbon molecules, ions, and clusters*, Chemical Reviews, **89**, 1713, 1989.

10. Cernicharo, J., Goicoechea, J. R. and Caus, E., *Far-infrared Detection of C_3 in Sagittarius B2 and IRC +10216*, Astrophysical Journal –Letters, **534**, L 117, 2000.

11. Kiess, N. H., and Bass, A.M., *The λ4050 group of the Cometary spectra in the Acetylene-Oxygen Flame,* Journal of Chemical Physics, **22**, 569, 1954.

12. van Orden, A. and Saykally, R. J., *Small Carbon Clusters: Spectroscopy, Structure, and Energetics*, Chemical Reviews, **98**, 2313, 1998.

13. Rohlfing, E.A., Goldsmith, J.E.M., *Stimulated-emission pumping spectroscopy of jet-cooled C_3: antisymmetric stretch-bend levels,* Journal of Optical Society of America B, **7**,1915, 1989.

14. Leider, H.R., Krikorian, O.H. and Young, D.A., *Thermodynamic properties of carbon up to the critical point*, Carbon, **11**, 555, 1973.

15. Rohlfing, E.A., *Laser-induced-fluorescence spectroscopy of jet-cooled C_3,* Journal of Chemical Physics, **91**, 4531, 1989.

16. Rousselot, P., Arpigny, C., Rauer, H., Cochran, A.L., Gredel, R., Cochran, W. D., Manfroid, J. and Fitzsimmons, A. *A fluorescence model of the C_3 radical in comets*, Astronomy and Astrophysics, **368**, 689, 2001.

17. Baker, J., Bramble, S. K. and Hamilton, P.A., *Observation of New Bands in the A $^1\Pi_u$ – X $^1\Sigma_g^+$ Laser Induced Fluorescence Spectrum of C_3,* Journal of Molecular Spectroscopy, **183**, 6, 1997.

18. Baker, J., Bramble, S. K. and Hamilton, P.A., *A hot band LIF study of the A $^1\Pi_u$-X $^1\Sigma_g^+$ transition in C_3,*.Chemical Physics Letters, **213**, 297, 1993.

19. Gausset, L., Herzberg, G., Lagerqvist, A. and Rosen, B. *Analysis of the 4050-Å group of the C_3 molecule*, Astrophysical Journal, **142**, 45, 1965.

20. Bengtsson, P.-E., Aldén, M., *Soot-visualization strategies using laser techniques – Laser-induced fluorescence in C_2 from laser-vaporized soot and laser-induced soot incandescence,* Applied Physics B, **60**, 51, 1995.

21. Ortman, B. J., Hauge, R.H. and Margrave, J.L., *Chemical reactions of carbon atoms and molecules from laser-induced vaporization of graphite, TaC and WC*, Journal of quantitative spectroscopy & radiative transfer, **40**, 439, 1988.

22. Nelson, H.H., Pasternack, L., Eyler, J.P. and McDonald, J.R., *Reactions of C_3 with alkenes, alkynes and allenes*, Chemical Physics, **60**, 231, 1981.

23. Nelson, H.H., Helvajian, H., Pasternack, L. and McDonald, J.R., *Temperature dependence of C_3 (X $^1\Sigma_g^+$) reactions with alkenes and alkynes,* Chemical Physics, **73**, 431, 1982.

24. Jensen, D. E., *Prediction of Soot Formation Rates: A New Approach*, Proceedings of the Royal Society of London. Series A., **338**, 375, 1974.

25. Northrup, E.J. and Sears, T. J., *Stimulated-emission pumping spectroscopy study of jet-cooled C_3: pure bending levels and bend-symmetric-strecth combination levels of X $^1\Sigma_g^+$*, Journal of the Optical Society of America B, **1924**, 7,1989.

26. Herzberg, G., *Molecular spectra and Molecular structure – II. Infrared and raman spectra*, D. Van Nordstrand Company Inc.: 1960.

27. Atkins, P. W., *Molecular quantum mechanics,* Clarendon P.: 1983.

28. Izuha, M. and Yamanouchi, K., *New $\tilde{A}$–$\tilde{X}$ vibronic bands of laser-vaporized C_3*, Journal of Chemical Physics, **109**, 1810, 1998.

29. Chang, K.W. and Graham, W. R. M. *Vacuum UV spectrum of C_3 trapped in argon at 8 K*, Journal of Chemical Physics, **77**, 4300, 1982.

30. Hwang, C. H., Klassen, S.A., Moazzen-Ahmadi N. and Tokaryk D.W., *Infrared diode laser spectroscopy of C_3: the ν_3 band of the a $^3\Pi_u$ electronic state*, Chemical Physics Letters, **250**, 273, 1996.

31. Tokyrak, D. W. and Chomiak, D.E., *Laser spectroscopy of C_3: Stimulated emission and absorption spectra of the A $^1\Pi_u$ – X $^1\Sigma_g^+$ transition*, Journal of Chemical Physics, **106**, 7600, 1997.

32. Izhua, M. and Yamanouchi, K., *Severely perturbed vibrational structure in the 266-310 nm electronic transition of C_3,* Journal of Chemical Physics, **113**, 10999, 2000.

33. Izuha, M. and Yamanouchi, K., *New vibronic bands of the laser-vaporized C_3 cluster. Determination of the ν_3 fundamental in the A $^1\Pi_u$ state***,** Chemical Physics Letters**, 242**, 435, 1995.

34. Kawaguchi, K., Matsumura, K., Kanamori, H. and Hirota, E., *Diode laser spectroscopy of C_3: The $\nu_2+\nu_3$, $2\nu_2+\nu_3-2\nu_2$, and $2\nu_2+\nu_3$ bands*, Journal of Chemical Physics, **91**, 1953, 1989.

35. Balfour, W. J., Jianying, C., Prasad, C.V.V. and Qian, C.X.V. *Laser-induced fluorescence spectroscopy of the A $^1\Pi_u$-X $^1\Sigma_g^+$ transition in jet-cooled C_3*,, Journal of Chemical Physics, **101**, 10343, 1994.

36. Herzberg, G., *Molecular spectra and Molecular structure – III. Electronic spectra and electronic structure of polyatomic molecules,* D. Van Nordstrand Company Inc.: 1966.

37. Weltner Jr, W. and McLeod Jr, D., *Spectroscopy of Carbon Vapor Condensed in Rare-Gas Matrices of 4° and 20° K. II*, Journal of Chemical Physics, **40**, 1305, 1964.

38. Civiš, S. and Tokaryk, D.W., *Fourier transform emission spectroscopy of triplet $^{13}C_3$*, Journal of Molecular Spectroscopy, **172**,543, 1995.

39. Sasada, H, Amano, T, Jarman, C. and Bernath, P. F., *A new triplet band system of C_3..The b $^3\Pi_u$-a $^3\Pi_u$ transition,* Journal of Chemial Physics, **94**, 2401, 1991.

40. Monninger, G., Förderer, M. , Gürtler, P., Kalhofer, S., Petersen, S., Nemes, L., Szalay, P. G. and Krätschmer, W., *Vacuum Ultraviolet Spectroscopy of the Carbon Molecule C_3 in Matrix Isolated State: Experiment and Theory,* Journal of Physical Chemistry A, **106**, 5779, 2002.

41. Lamire, G. W., Fu, Z., Hamrick, Y.M., Taylor, S. and Morse, M.D., *New electronic band systems of jet-cooled carbon trimer: 266-302 nm*, Journal of Physical Chemistry, **93**, 2313, 1989.

42. Eckberth, A. C., *Laser Diagnostics for Combustion Temperature and Species,* Plenum Publisching Corporation: 1996.

43. Svelto, O, *Principles of Lasers,* Gordon and Breach Publischers: 1998.

44. Petterson, S.-G., Borgström, S. and Hertz, H., *Optisk teknik/ Advanced Optics,* lecture notes, 1999.

45. Cooper, D.M. and Jones, J.J, *An experimental determination of the cross section of the swings band system of C_3,* Journal of Quantitative Spectroscopy and Radiative Transfer, **22**, 201, 1979.

46. Mebel, A. M. and Kaiser, R. I., *An ab initio study on the formation of interstellar tricarbon isomers l-C_3 ($X^1\ \Sigma_g^+$) and c-C_3 ($X^3\ A_2'$)*, Chemical Physics Letters, **360**, 139, 2002.